Published in final edited form as:

Leukemia. 2020 January ; 34(1): 138–150. doi:10.1038/s41375-019-0503-z.

Targeting Translation Initiation by Synthetic Rocaglates for Treating MYC-driven Lymphomas

Xuan Zhang[*,1], **Chengfeng Bi**[*,1], **Ting Lu**[1], **Weiwei Zhang**[1], **Ting Yue**[1], **Cheng Wang**[1], **Tian Tian**[1], **Xiaoyan Zhang**[1], **Yuhua Huang**[1], **Matthew Lunning**[1], **Xinbao Hao**[3], **Lauren E. Brown**[2], **William G. Devine**[2], **Julie Vose**[1], **John A. Porco Jr.**[2], **Kai Fu**[1]

[1]Departments of Pathology, Hematology and Oncology, Fred & Pamela Buffett Cancer Center, University of Nebraska Medical Center, Omaha, Nebraska

[2]Center for Molecular Discovery (BU-CMD), Boston University, Boston, Massachusetts

[3]Departments of Hematology and Pathology, Sino-US lymphoma Center, Hainan Medical University First Affiliated Hospital, Haikou, Hainan, China

Abstract

MYC-driven lymphomas, especially those with concurrent MYC and BCL2 dysregulation, are currently a challenge in clinical practice due to rapid disease progression, resistance to standard chemotherapy and high risk of refractory disease. MYC plays a central role by coordinating hyperactive protein synthesis with upregulated transcription in order to support rapid proliferation of tumor cells. Translation initiation inhibitor rocaglates have been identified as the most potent drugs in MYC-driven lymphomas as they efficiently inhibit MYC expression and tumor cell viability. We found that this class of compounds can overcome eIF4A abundance by stabilizing target mRNA-eIF4A interaction that directly prevents translation. Proteome-wide quantification demonstrated selective repression of multiple critical oncoproteins in addition to MYC in B cell lymphoma including NEK2, MCL1, AURKA, PLK1, and several transcription factors that are generally considered undruggable. Finally, (−)-SDS-1–021, the most promising synthetic rocaglate, was confirmed to be highly potent as a single agent, and displayed significant synergy with the BCL2 inhibitor ABT199 in inhibiting tumor growth and survival in primary lymphoma cells in *vitro* and in patient-derived xenograft mouse models. Overall, our findings support the strategy of using rocaglates to target oncoprotein synthesis in MYC-driven lymphomas.

Keywords

MYC-driven lymphoma; double hit lymphoma; translation initiation; rocaglate; (-)-SDS-1-021; eIF4A

Corresponding Author: Dr. Kai Fu, University of Nebraska Medical Center, MSB 3522, S 42nd St & Emile St, Omaha, NE 68198, USA, Tel: 402-559-7526, Fax: 402-559-6018, kfu@unmc.edu.

*X.Z. and C.B. contributed equally to this study.

Conflict-of-interest

The authors declare no competing financial interests.

Introduction

MYC aberrations including translocation and amplification are commonly observed in B cell lymphomas. As a result, overexpressed MYC serves as the driving force in disease transformation and progression(1) through differentially regulating target genes(2), as well as enhancing existing oncogenic pathway activities(3). While *MYC* rearrangements characterize Burkitt lymphoma (BL), they are also present in ~15% of diffuse large B cell lymphomas (DLBCL) and are found to be associated with inferior outcomes (4–6). Notably, the majority of *MYC* translocated DLBCL also possesses the *IGH/BCL2* rearrangement(7), comprising the category "high-grade B-cell lymphoma with translocations involving *MYC* and *BCL2* and/or *BCL6*" in 2016 WHO classification (double-hit or triple-hit lymphoma; DHL/THL)(8). Cases with concomitant overexpression of MYC and BCL2 proteins, which represent a larger group characterized as "immunohistochemical double-hit lymphomas" (double expression lymphomas, DEL)(9), appear to have a similar clinical course. Generally, DHL/DEL accounts for about 30% of aggressive B-cell lymphomas and is highly aggressive with the median overall survival ranging from less than 12 months with standard R-CHOP therapy (10, 11).

Given the central role MYC plays in aggressive B cell lymphomas, several strategies were proposed to target this "undruggable" transcription factor, such as disrupting MYC transcription by bromodomain (BRD)-4 inhibitors. However, early clinical data showed that BRD4 inhibitors failed to provide durable cytotoxic effects in human cancers as a single agent(12). Reversal of MYC inhibition was found among relapsed patients (13), and reactivation of multiple oncogenic pathways was detected in BRD4 inhibitor-resistant cells (14, 15). While transcription adaption and reprogramming are prone to occur during tumor evolution, which is largely the cause of failure for single target inhibitors, augmented protein synthesis following MYC activation is always required to accommodate rapid proliferation, and has been demonstrated to be a rate-limiting determinant of cancer development(16). As a result, targeting protein synthesis may provide an effective and lasting approach for treating MYC-driven lymphomas(17).

Translation initiation is the rate-limiting step in protein sythesis, and is tightly controlled by interactions of the mRNA 5'UTR with initiation factors in a cap-dependent manner, or, less commonly, in a cap-independent manner by internal ribosome entry site (IRES). Many oncogenes such as *MYC* and *CCND1* possess complex secondary structures on the mRNA 5'UTR which rely heavily on cap-dependent initation for efficient translation(18, 19). On the other hand, MYC directly induces expression of components of the eukaryotic initiation factor 4F (eIF4F) complex and activates the mammalian target of rapamycin (mTOR) signaling(20), consequently upregulating cap-dependent translation initiation(21). Therefore, strategies directed against translation initiation are able to disrupt both MYC expression and the hyperactivated translation that it causes(17).

Rocaglates, a class of natural products isolated from plants of the *Aglaia* genus, are currently the most potent class of translation initiation inhibitors that function *via* eIF4A and are well tolerated *in vivo* (22–25). Several rocaglates including silvestrol and rocaglamide have showed selective inhibition of multiple oncoproteins such as MYC and MCL1, and have

exhibited a remarkable cytotoxic effect on a variety of tumors both *in vitro* and *in vivo* (23, 25–27). Herein, we identified that translation initiation inhibitors are strong candidates for treating MYC-driven B cell lymphomas, and demonstrated the advantage of rocaglates *vs.* mTOR inhibitors on the inhibition of MYC expression. Moreover, we studied the mechanism of rocaglate therapy and identified multiple B cell-related oncoproteins being depleted. Finally, we demonstrated the therapeutic efficacy of the most potent rocaglate derivative (–)-SDS-1–021 *in vitro* and in patient-derived xenograft (PDX) models.

Materials and Methods

Tandem mass tag based mass spectrometry (TMT-MS)

Val cells were treated with (-)-SDS-1-021 (100 nM) or vehicle control for 4 hours. Proteins were extracted using radioimmunoprecipitation (RIPA) assay buffer with proteinase and phosphatase inhibitor cocktail. Proteins from three biological replicates were labeled using 6-plex TMT kit (Thermo Fisher Scientific, Waltham, MA, USA) according to manufacturer's protocol and then pooled together and fractionated by high-pH reverse phase chromatography. Dried fractions were re-dissolved and run by nano-LC-MS/MS using a 2-hour gradient on a 0.075 mm x 250 mm C18 Waters CSH column feeding into a Q-Exactive HF mass spectrometer (Thermo Fisher Scientific).

In vivo patient-derived xenograft

Approximately 10^6~5×10^6 DEL/DHL cells from second passage PDX were inoculated to the flank of 6–8 week old NSG mice (JAX lab, Bar Harbor, ME, USA). After tumor reached palpable size, tumor-bearing mice were separated into vehicle control group (5.2% Tween 80/5.2% PEG400 in water) and (-)-SDS-1-021 group (0.2 mg/kg). An additional ABT199 group (1.0 mg/kg) and a combined treatment group ((-)-SDS-1-021 0.2 mg/kg + ABT199 1.0 mg/kg) were added for DHL model. Each group contained six mice with an equal number of male and female animals. Drug or vehicle was given ip daily for 10 consecutive days. Animals were weighted and tumor size was measured with caliper daily. Tumor volume was calculated as $V = (W^2 \times L)/2$. At day 10 or endpoint, mice were euthanized, and the tumor was isolated for further examinations.

Additional information can be found in "supplementary materials and methods".

Results

Inhibitors targeting translation initiation exhibit high potency in MYC-driven lymphomas

To identify candidate drugs for MYC-driven lymphoma, imaging- and stroma-based drug screening assays utilizing 30 small molecule inhibitors targeting the major signaling pathways in B cell lymphoma were conducted in 11 aggressive MYC-driven B cell lymphoma cell lines, including three BL (Namalwa, Raji and Ramos) wild-type or with isogenic BCL2 expression, four DHL/DEL CJ, Val, Dohh2, U2932, and the mantle cell lymphoma line Sp53. Among tested inhibitors, the rocaglate silvestrol exhibited the highest potency across all tested cells followed by the mTOR inhibitors AZD8055 and BEZ235, the PI3K inhibitor PIK75, and the PLK1 inhibitor Volasertib (Figure 1A). To validate our

results, we performed a viability assay in three DHL cells treated with silvestrol and AZD8055 at various concentrations and found that although both drugs act on translation initiation, tested cells are much more sensitive to silvestrol (Figure 1B). Overall, our data suggest that targeting mRNA translation initiation is a promising strategy in MYC-driven lymphomas.

Rocaglates but not mTOR inhibitors efficiently repress MYC expression

We next studied the effect of translation initiation inhibitors on MYC expression, given its central role in MYC-driven lymphoma. mTOR complex 1 (mTORC1) is the major sensor of nutrition and master regulator of growth in eukaryotic cells with two primary downstream targets, S6 kinase 1 (S6K1) and eukaryotic translation initiation factor 4E-binding protein 1 (4EBP1). mTORC1 promotes translation initiation by phosphorylating 4EBP1. Phosphorylated 4EBP1 dissociates from eIF4E thereby allowing the formation of the eIF4F complex. To evaluate the effect of mTOR inhibitors on MYC expression, we treated the DHL cell lines Val and Ros50 with both allosteric and kinase inhibitors of mTOR. As expected, the mTOR kinase inhibitors (TORKi) Torin1 and AZD8055 dramatically decreased the activity of S6K1 as shown by the phosphorylation of downstream substrate ribosomal protein s6 (RPS6) as well as the phosphorylation 4EBP1, whereas the allosteric inhibitor temsirolimus failed to completely inhibit 4EBP1. Surprisingly, the TORKis only marginally affected MYC expression in both cell lines, while the expression of another cap-dependent oncoprotein MCL1 was significantly decreased (Figure 2A). To confirm these results, we employed the 4EBP1 mutant, 4EBP1–4A as a dominant cap-dependent translation initiation inhibitor(28). 4EBP1–4A carries alanine substitutions at four serine/threonine residues and thereby prevents dissociation of 4EBP1 from eIF4E induced by mTORC1. Interestingly, MYC expression was unchanged upon ectopic expression of the doxycycline-inducible 4EBP1–4A in both DHL cells (Figure 2B). Since both TORKi- and 4EBP1–4A repress cap-dependent translation through sequestering eIF4E, such indirect inhibitory effect is determined by the eIF4E/4EBP1 ratio. We then disrupted eIF4E by siRNA knockdown and observed a substantial decrease in MYC expression (Figure 2C) suggesting that excessive abundance of eIF4E may have compromised the effect of TORKi on cap-dependent translation. Consistent with this finding, slight to moderate suppression of eIF4E using increasing doses of the putative eIF4E inhibitors briciclib or 4EG-I was unable to efficiently repress MYC expression (Figure S1A and S1B). These data indicate that cap-dependent translation is crucial for MYC mRNA translation. However, since eIF4E is highly abundant in lymphocytes and eIF4E overexpression is commonly observed in B cell malignancies (29), TORKi treatment is insufficient to overcome the abundance of eIF4E and suppress MYC expression in MYC-driven lymphomas.

In contrast, silvestrol treatment dramatically decreased MYC expression in DHL and DEL cells (Figure 2D) at 5 nM, and abolished MYC expression at higher biologically relevant concentrations. Moreover, we tested silvestrol in P493–6 cells in which MYC expression is tetracycline-repressible, and found low concentration of silvestrol was able to abrogate MYC expression comparable to doxycycline (Figure S1C). Furthermore, silvestrol exhibited more potent inhibition of MCL1 expression compared to TORKi, yet neither significantly decreased BCL2 in DHL cells (Figure 2A and 2D). The findings are consistent with the fact

that MCL1 has a short half-life and as such any subtle change in protein synthesis or degradation would greatly affect the protein level, whereas the BCL2 protein is stable with a half-life of approximate 20 hours (30, 31). Taken together, we demonstrated that silvestrol potently repressed MYC expression in all MYC deregulated B cell lymphoma lines; however the inhibitory effect of mTOR inhibitors was compromised due to eIF4E overexpression.

Rocaglate strongly inhibits the cap-dependent translation of MYC

To provide insight into the distinct impact of TORKi and rocaglates on mRNA translation, we performed polysome fractionation to further analyze the mRNA distribution on ribosomes (Figure 2E). We found that silvestrol induced stronger overall translational suppression than Torin1 in both Val and Ros50 cells as indicated by the elevated 80S monosome peak and the declined polysome peaks. We then assessed the abundance of MYC mRNA in each fraction and observed redistribution from actively translating polysomes to lighter fractions in silvestrol-treated cells (Figure 2F). Similarly, the redistribution of BCL2 and MCL1 mRNA was more prominent upon silvestrol administration. These findings are in accordance with the observation that silvestrol has greater impact on protein synthesis, especially for MYC. Because MYC mRNA contains an IRES element in 5'UTR, which provides MYC translation with an alternative mode of initiation, we then sought to determine if both cap- and IRES-dependent translations were affected. To measure the activities of cap- and IRES-dependent translation respectively, we generated two dual luciferase reporter constructs: pURF with insertion of the IRES-deleted MYC-5'UTR upstream of renilla luciferase, and pURF-IRES with the addition of MYC-IRES to drive translation of firefly luciferase (Figure 2G). We first transfected these constructs into 293T cells and then treated the cells with either silvestrol or Torin1 (Figure S2). As expected, firefly luciferase expression was exponentially increased in pURF-IRES transfected cells. Both cap- and IRES-dependent translations were decreased by either silvestrol or Torin1 treatment as indicated by renilla and firefly activity respectively. However, silvestrol displayed much stronger inhibition, especially for cap-dependent translation. Next, we stably transduced DHL cells with the dual luciferase reporters using retrovirus and observed similar results as those in 293T cells (Figure 2H). Particularly, with silvestrol treatment, renilla activity was reduced by 37% and 35% at 25 nM in Val and Ros50 cells, respectively, and by ~55% and ~44% at 125 nM. By contrast, firefly activity was only moderately decreased with silvestrol treatment and was even less affected upon Torin1 administration. Since 25 nM of silvestrol was sufficient to abolish MYC expression whereas even 200 nM of Torin1 only showed marginal effect (Figure 2A and 2D), these findings suggest that the potent inhibition of MYC by rocaglates is mainly mediated by the substantial repression of cap-dependent translation, although both cap and IRES dependent translations are affected(32, 33).

Rocaglates overcome eIF4A abundance

Previous studies have disclosed rocaglates as selective inhibitors of eIF4A through diminishing its availability in eIF4F complex (25, 26, 34, 35), however recent evidence demonstrated that rocaglates directly bind at the interface formed between eIF4A and polypurine sequences on targeted mRNA, forming a stable structure to prevent ribosome

scanning(36, 37). Herein, we were interested to determine through which mechanism rocaglates achieved efficient MYC repression in DHL/DEL. First we probed the expression of eIF4A in DHL/DEL cells. The eIF4A family consists of three helicases in which eIF4A1 and eIF4A2 share high resemblance and were reported to interact with silvestrol and episilvestrol(38), whereas eIF4A3 is distant from these isoforms in both amino acid sequence and function(39). We found that eIF4A1 but not eIF4A2 is highly up-regulated in DHL/DEL cells as compared to normal B cells (Figure S3A). Consistently, eIF4A1 mRNA was found to be much more abundant than eIF4A2 (Figure S3B), and knockdown of eIF4A1, but not eIF4A2, had significant impact on cell viability (Figure S3C). These data are in accordance with the common notion that eIF4A1 is the major helicase required in cancers.

Next, we compared the impact of eIF4A knockdown (Figure 3A) versus rocaglate treatment (Figure 3B) in two aspects, eIF4A abundance in eIF4F and MYC expression. Following siRNA-mediated eIF4A1 knockdown, consistent with previous reports (40, 41), we observed a marked increase of eIF4A2 expression while eIF4A1 showed no changes to eIF4A2 depletion (Figure 3A and 3C). m^7GTP pull-down assay confirmed depletion of eIF4A1 and eIF4A2 in the eIF4F complex in single knockdown cells. eIF4A½ double knockdown significantly decreased eIF4A abundance in eIF4F complex in Ros50, however such reduction is not as prominent in Val (Figure 3A), as reduced eIF4A may still be more abundant than the relatively low level of eIF4E in this cell line (Figure S3A). Cell viability assay confirmed that Ros50 is more vulnerable to eIF4A depletion than Val (Figure S3C). We then analyzed MYC expression upon eIF4A knockdown and were surprised to find that the MYC protein level was only marginally decreased in these cell lines (Figure 3C). Dual luciferase assay revealed that eIF4A knockdown failed to induce comparable reduction of luciferase activity (Figure 3D) to silvestrol treatment as shown in Figure 2H. These findings suggest that eIF4A1 is highly abundant in MYC-driven lymphoma wherein even up to 70% depletion had minimal effect on MYC translation. In contrast, the abundance of eIF4A1 and eIF4A2 in the eIF4F complex was barely affected by a high concentration of silvestrol or (-)-SDS-1-021, a synthetic rocaglate that is more potent as a translation inhibitor than silvestrol(23, 42) (Figure 3B and S4). Unlike eIF4A knockdown, rocaglates efficiently repressed MYC at a low concentration (Figure 2D), and had no additive effect with eIF4A knockdown in repressing MYC (Figure 3C). In addition, rocaglates appeared to be much more effective on MYC repression than hippuristanol, an ATP-competitive inhibitor of eIF4A which impairs its helicase function (Figure 3E). These findings suggest that the potent MYC suppression by rocaglates is unlikely a consequence of eIF4A depletion in eIF4F complex in MYC-driven lymphoma cells.

Finally, to test whether rocaglates directly alter eIF4A and MYC mRNA binding, we conducted native RNA immunoprecipitation (RIP). We found MYC mRNA was significantly enriched on eIF4A1 and eIF4A2 upon rocaglate treatment (Figure 3F), while the previously described rocaglate-insensitive mRNA NDUFS7 was not (37) (Figure S5), suggesting that the rocaglate selectively stabilized the eIF4A-MYC mRNA interface. It has been shown that the eIF4A-mRNA-rocaglate structure is very stable that may persist even after ATP hydrolysis, therefore directly prevents ribosome scanning in translation initiation (36, 37). Collectively, we demonstrated that eIF4A exists in excess in MYC-driven

lymphoma cells, and that moderate depletion is insufficient to repress MYC translation. Apparently, rocaglates efficiently repress MYC translation by increasing MYC mRNA binding to eIF4A, instead of depleting it in eIF4F complex, and therefore overcome eIF4A abundance.

Rocaglates repress multiple critical oncoproteins in MYC-driven lymphoma

To better characterize the translation inhibitory effect of rocaglates in DHL, we performed tandem mass tag-based mass spectrometry (TMT-MS) to quantitatively delineate proteome-wide changes. In Val cells treated with (-)-SDS-1-021 for 4 hours, the total abundance of 177 proteins was depleted more than 20% ($p<0.05$) (Figure 4A and S6A), among which multiple oncoproteins critical for B cell lymphomagenesis were identified (Figure 4A). Pathway enrichment analysis revealed that cell cycle and PLK1 pathway activity were mostly involved (Figure 4B and S6B).

Notably, the Aurora-PLK-1 pathway kinases, including NEK2, AURKA, AURKB, PLK1, WEE1, and CHEK1 were highly enriched in the depleted protein pool. This group of kinases is commonly recognized as checkpoint regulators, whereas emerging evidence revealed their essential role in cancer development, especially in maintaining MYC functions (43, 44). These data highly suggest that not only MYC expression but also its functional network was impaired by rocaglate treatment. In addition, we noticed that besides MYC, multiple B cell lymphoma-related transcription factors were also significantly decreased, including EST1, TCF3, BCL6, and NOTCH1, which greatly enhanced the therapeutic value of rocaglates, given that transcription factors are usually hard to target using small molecule inhibitors. Also, we examined the total (Figure S6C) and eIF4A-bound mRNA levels (Figure S5) of the representative depleted genes and found that most of them were up-regulated and enriched on eIF4A upon rocaglate treatment, suggesting that the depletion indeed resulted from translation inhibition. We then validated the results in four DHL/DEL cell lines and found that different from Torin1 treatment (Figure S6D), all of the examined oncoproteins were consistently depleted by silvestrol and (-)-SDS-1-021 at relatively low concentration (25 nM) (Figure 4C). Overall, these findings suggest that rocaglates and derivatives bear great potential for treating MYC-driven lymphomas due to the collaborative inhibition of MYC as well as multiple critical B cell lymphoma-associated oncoproteins.

(-)-SDS-1-021 exhibits promising therapeutic effect, and synergizes with ABT199 *in vitro* and *in vivo*

As shown in Figure 2, neither TORKi nor silvestrol were able to repress BCL2 expression in DHL cells, likely due to its high abundance and long half-life. Therefore, we tested whether the addition of BCL2 inhibitor ABT199 may synergize with rocaglates for more efficient tumor suppression. Val and Ros50 cells were treated with silvestrol and ABT199 at various concentrations, individually or in combination (Figure S7A). As expect, single treatment induced slight-to-moderate cell death, while the combined treatment exhibited significant synergy and dramatically killed the lymphoma cells. Next, we found that (-)-SDS-1-021 showed a strong inhibitory effect at a very low concentration (2.5 nM) especially in DHL/DEL lymphoma cells (Figure S7B, Figure 5A and 5B). Importantly, CD19-positive normal B cells showed relative resistance to (-)-SDS-1-021 treatment (Figure 5A), in

agreement with our finding that multiple lymphoma- related oncoproteins are repressed by rocaglates. We then employed (-)-SDS-1-021 and combination treatment in a series of primary DEL/DHL cells and found (-)-SDS-1-021 potently decreased cell viability whilst the inhibitory effect was further enhanced when combined with ABT199 (Figure 5C).

To assess the *in vivo* therapeutic effect, we adopted two established PDX models, one derived from a DEL patient and the other derived from a relapsed DHL patient. For the DEL model, single treatment of (-)-SDS-1-021 at a low dosage of 0.2 mg/kg was sufficient to abolish tumor growth and eliminated the tumor burden in these animals (Figure 5D-F). The DHL model exhibited more aggressive behaviors with expeditious tumor growth, blood vessel infiltration and local invasion. ABT199 single treatment was able to moderately delay tumor growth. By contrast, (-)-SDS-1-021 single treatment induced potent tumor repression while the combination with ABT199 almost abolished the tumor burden with only minimal residuals observed at the implanted site (Figure 5G-I). Morphological and immunohistochemical examination revealed that (-)-SDS-1-021 treatment induced massive cell death, substantially decreased cell proliferation and abrogation of MYC expression in DEL PDX model (Figure 5J). In DHL PDX model, ABT199 single treatment had no effect on MYC expression or proliferative index. (-)-SDS-1-021 administration substantially decreased MYC expression (>50% in controls vs 10% in (-)-SDS-1-021 group vs <5% in combination group) and ki67 index (100% in controls vs ~40% in (-)-SDS-1-021 group vs ~20% in combination group) (Figure 5J). No significant body weight loss or emaciation was observed in treatment groups. These findings strongly suggest that (-)-SDS-1-021 is a promising therapeutic reagent which may synergize with ABT199 for the treatment of MYC-driven lymphomas.

Discussion

In MYC-driven lymphomas, protein synthesis is enhanced to sustain rapid proliferation through MYC-mediated upregulation of eIF4E, eIF4A, and eIF4G (45). Upregulated translation, in turn, promotes excessive production of MYC, thereby forming a feed-forward loop between MYC and active mRNA translation(46). As a result, targeting protein synthesis, especially initiation through components of the eIF4F complex, has great potential. Indeed, our drug screen identified translation inhibitors to exhibit the highest potency across tested MYC-driven lymphoma cells. However, the highly overexpressed eIF4F complex components in MYC-driven lymphoma, especially eIF4E and eIF4A, may compromise the efficacy of direct inhibitors. Consistent with previous reports (47), we demonstrated that overexpressed eIF4E weakened the effect of cap-dependent translation inhibition and sustained MYC expression upon mTOR inhibitors, bircicilib or 4EG-I treatment. Unlike mTOR inhibitors, rocaglates potently represses MYC translation, as indicated by strong inhibition of cap-dependent translation. It is interesting that targeting eIF4A would generate such efficient repression on MYC, as eIF4A is the most abundant initiation factor whereas eIF4E is the least abundant one(41, 48). In fact, we showed eIF4A exists in excess in DHL cells that moderate depletion may not be able to suppress MYC expression. Moreover, we found rocaglates did not change the total level of eIF4A or deplete it within eIF4F complex, instead increasing the binding of target mRNA on eIF4A. Recent studies have clarified rocaglates as a type of interfacial inhibitors that bind to the pocket

formed by eIF4A and polypurine-rich mRNA, functioning as a roadblock against translation(36, 37).This unique action allows rocaglates to take advantage of the overly abundant eIF4A in MYC-driven lymphoma thereby effectively repressing MYC and other target mRNA translation, meanwhile inhibitors targeting eIF4A function, e.g. hippuristanol and elatol, struggle to saturate the gigantic eIF4A pool and often exhibit low potency(49, 50).

We found oncoproteins depleted by rocaglates in DHL principally consist of two major categories, proliferation-related kinases and transcription factors. The proliferation-related kinases predominantly reside in the replication checkpoint Aurora-PLK1 signaling and downstream targets. These kinases control the progression from G2 to M phase meanwhile play an important role in maintaining the stability of MYC protein (43, 44). As a result, rocaglates not only potently repress MYC but also simultaneously disrupt the MYC regulatory network, again highlighting this class of compounds as a promising candidate for treating MYC driven lymphomas. Transcription factors in addition to MYC, such as TCF3, BCL6 and NOTCH1 play crucial roles in the B cell lymphomagenesis (51–54) and were also substantially suppressed by rocaglate treatment. This finding implies a great therapeutic value in lymphoma treatment, as transcription factors usually have wide active domains that are unable to be targeted by small molecule inhibitors. Collectively, in light of their multi-targeting properties, rocaglates should be considered as a broad-spectrum therapeutic agent, which has many virtues such as high potency and a lower likelihood for the resistance development.

Although rocaglates exhibited potent inhibition on MYC and other oncoproteins, BCL2, the hallmark anti-apoptotic protein overexpressed in DHL/DEL remains unaffected. Therefore, the combination of ABT199 with rocaglates showed a remarkable synergistic effect which may result from simultaneous inhibition of BCL2 and MCL1 according to our previous study (55). The combination strategy significantly decreased the effective dosage of both rocaglate and ABT199, and thus could minimize the toxicity of both drugs.

Finally, large scale chemical synthesis of rocaglate derivatives has been achieved recently (56), and hence the limited availability from natural resources (e.g. silvestrol) will no longer hinder potential use of this class of inhibitors. Our previous compound screen unveiled a few synthetic rocaglates that are especially promising including CR-1–31-B and (-)-SDS-1-021(57–59). In the present study, a low dose (0.2 mg/kg) of (-)-SDS-1-021 is sufficient to induce rapid tumor regression in DHL/DEL PDX mouse models, which is consistent with the previous study showing high potency of this compound in multiple myeloma *in vivo*(23). Taken together, the preclinical findings presented here demonstrate that synthetic rocaglates are promising candidates for treating aggressive B cell lymphoma, especially for the most refractory type DHL/DEL. Despite silvestrol showing favorable pharmacokinetics in mice (60), the pharmacokinetics and pharmacodynamics of rocalgate derivate such as (-)-SDS-1-021 should be further characterized before they are taken into clinical trials.

Supplementary Material

Refer to Web version on PubMed Central for supplementary material.

Acknowledgments

We would like to thank Jerry Pelletier at the McGill University for his valuable advice and comments to the manuscript. We thank Joseph Gera (Greater Los Angeles VA Healthcare System, CA, USA) for provide us pRF plasmid. We thank Dirk Eick (Helmholtz Zentrum München, Munich, Germany) for providing us P493-6 cell line. We thank John Chang (City of Hope, CA, USA) for providing NKYS cell line. We thank Richard J. Ford (MD. Anderson, TX, USA) for providing CJ cell line. We thank We thank Sophie Alvarez and Michael Naldrett at the Proteomics and Metabolomics Facility, Nebraska Center for Biotechnology, University of Nebraska-Lincoln, supported by the Nebraska Research Initiative for performing the proteomics analysis. We sincerely thank Wang Yuzhuo (Vancouver, British Columbia) at the Living Tumor Laboratory for providing MYC/BCL2 double expression PDX model. We thank David M. Weinstock and Dana-Farber's bank of patient-derived tumor xenografts (Dana-Farber Cancer Institute, MA, USA) for providing the MYC/BCL2 double translocation PDX line. This study was supported in part by a pilot grant and a lymphoma program grant from the Fred & Pamela Buffett Cancer Center at UNMC (to KF), the National Cancer Institute (P30 CA036727), Nebraska Department of Health and Human Services (LB506-18-22 to KF), and the National Institutes of Health (R35 GM118173 and R24 GM111625 to J.A.P., Jr.).

Acknowledgement of research support for the study:

This study was supported in part by a pilot grant and a lymphoma program grant from the Fred & Pamela Buffett Cancer Center at UNMC (to KF), the National Cancer Institute (P30 CA036727), Nebraska Department of Health and Human Services (LB506-18-22 to KF), and the National Institutes of Health (R35 GM118173 and R24 GM111625 to J.A.P., Jr.).

Reference

1. Ott G, Rosenwald A, Campo E. Understanding MYC-driven aggressive B-cell lymphomas: pathogenesis and classification. Blood. 2013;122(24):3884–91. [PubMed: 24009228]
2. Sabo A, Kress TR, Pelizzola M, de Pretis S, Gorski MM, Tesi A, et al. Selective transcriptional regulation by Myc in cellular growth control and lymphomagenesis. Nature. 2014;511(7510):488–92. [PubMed: 25043028]
3. Nie Z, Hu G, Wei G, Cui K, Yamane A, Resch W, et al. c-Myc is a universal amplifier of expressed genes in lymphocytes and embryonic stem cells. Cell. 2012;151(1):68–79. [PubMed: 23021216]
4. Scott DW, King RL, Staiger AM, Ben-Neriah S, Jiang A, Horn H, et al. High-grade B-cell lymphoma with MYC and BCL2 and/or BCL6 rearrangements with diffuse large B-cell lymphoma morphology. Blood. 2018;131(18):2060–4. [PubMed: 29475959]
5. Savage KJ, Johnson NA, Ben-Neriah S, Connors JM, Sehn LH, Farinha P, et al. MYC gene rearrangements are associated with a poor prognosis in diffuse large B-cell lymphoma patients treated with R-CHOP chemotherapy. Blood. 2009;114(17):3533–7. [PubMed: 19704118]
6. Barrans S, Crouch S, Smith A, Turner K, Owen R, Patmore R, et al. Rearrangement of MYC is associated with poor prognosis in patients with diffuse large B-cell lymphoma treated in the era of rituximab. J Clin Oncol. 2010;28(20):3360–5. [PubMed: 20498406]
7. Aukema SM, Siebert R, Schuuring E, van Imhoff GW, Kluin-Nelemans HC, Boerma EJ, et al. Double-hit B-cell lymphomas. Blood. 2011;117(8):2319–31. [PubMed: 21119107]
8. Swerdlow SH, Campo E, Pileri SA, Harris NL, Stein H, Siebert R, et al. The 2016 revision of the World Health Organization classification of lymphoid neoplasms. Blood. 2016;127(20):2375–90. [PubMed: 26980727]
9. Sarkozy C, Traverse-Glehen A, Coiffier B. Double-hit and double-protein-expression lymphomas: aggressive and refractory lymphomas. Lancet Oncol. 2015;16(15):e555–e67. [PubMed: 26545844]
10. Johnson NA, Savage KJ, Ludkovski O, Ben-Neriah S, Woods R, Steidl C, et al. Lymphomas with concurrent BCL2 and MYC translocations: the critical factors associated with survival. Blood. 2009;114(11):2273–9. [PubMed: 19597184]

11. Green TM, Young KH, Visco C, Xu-Monette ZY, Orazi A, Go RS, et al. Immunohistochemical double-hit score is a strong predictor of outcome in patients with diffuse large B-cell lymphoma treated with rituximab plus cyclophosphamide, doxorubicin, vincristine, and prednisone. J Clin Oncol. 2012;30(28):3460–7. [PubMed: 22665537]
12. Doroshow DB, Eder JP, LoRusso PM. BET inhibitors: a novel epigenetic approach. Ann Oncol. 2017;28(8):1776–87. [PubMed: 28838216]
13. Stathis A, Zucca E, Bekradda M, Gomez-Roca C, Delord JP, de La Motte Rouge T, et al. Clinical Response of Carcinomas Harboring the BRD4-NUT Oncoprotein to the Targeted Bromodomain Inhibitor OTX015/MK-8628. Cancer Discov. 2016;6(5):492–500. [PubMed: 26976114]
14. Pawar A, Gollavilli PN, Wang S, Asangani IA. Resistance to BET Inhibitor Leads to Alternative Therapeutic Vulnerabilities in Castration-Resistant Prostate Cancer. Cell Rep. 2018;22(9):2236–45. [PubMed: 29490263]
15. Kurimchak AM, Shelton C, Duncan KE, Johnson KJ, Brown J, O'Brien S, et al. Resistance to BET Bromodomain Inhibitors Is Mediated by Kinome Reprogramming in Ovarian Cancer. Cell Rep. 2016;16(5):1273–86. [PubMed: 27452461]
16. Barna M, Pusic A, Zollo O, Costa M, Kondrashov N, Rego E, et al. Suppression of Myc oncogenic activity by ribosomal protein haploinsufficiency. Nature. 2008;456(7224):971–5. [PubMed: 19011615]
17. Bhat M, Robichaud N, Hulea L, Sonenberg N, Pelletier J, Topisirovic I. Targeting the translation machinery in cancer. Nat Rev Drug Discov. 2015;14(4):261–78. [PubMed: 25743081]
18. Hinnebusch AG, Ivanov IP, Sonenberg N. Translational control by 5'-untranslated regions of eukaryotic mRNAs. Science. 2016;352(6292):1413–6. [PubMed: 27313038]
19. Topisirovic I, Svitkin YV, Sonenberg N, Shatkin AJ. Cap and cap-binding proteins in the control of gene expression. Wiley Interdiscip Rev RNA. 2011;2(2):277–98. [PubMed: 21957010]
20. Ravitz MJ, Chen L, Lynch M, Schmidt EV. c-myc Repression of TSC2 contributes to control of translation initiation and Myc-induced transformation. Cancer Res. 2007;67(23):11209–17. [PubMed: 18056446]
21. Elkon R, Loayza-Puch F, Korkmaz G, Lopes R, van Breugel PC, Bleijerveld OB, et al. Myc coordinates transcription and translation to enhance transformation and suppress invasiveness. EMBO Rep. 2015;16(12):1723–36. [PubMed: 26538417]
22. Lucas DM, Edwards RB, Lozanski G, West DA, Shin JD, Vargo MA, et al. The novel plant-derived agent silvestrol has B-cell selective activity in chronic lymphocytic leukemia and acute lymphoblastic leukemia in vitro and in vivo. Blood. 2009;113(19):4656–66. [PubMed: 19190247]
23. Manier S, Huynh D, Shen YJ, Zhou J, Yusufzai T, Salem KZ, et al. Inhibiting the oncogenic translation program is an effective therapeutic strategy in multiple myeloma. Sci Transl Med. 2017;9(389).
24. Pan L, Woodard JL, Lucas DM, Fuchs JR, Kinghorn AD. Rocaglamide, silvestrol and structurally related bioactive compounds from Aglaia species. Nat Prod Rep. 2014;31(7):924–39. [PubMed: 24788392]
25. Bordeleau ME, Robert F, Gerard B, Lindqvist L, Chen SM, Wendel HG, et al. Therapeutic suppression of translation initiation modulates chemosensitivity in a mouse lymphoma model. J Clin Invest. 2008;118(7):2651–60. [PubMed: 18551192]
26. Wiegering A, Uthe FW, Jamieson T, Ruoss Y, Huttenrauch M, Kuspert M, et al. Targeting Translation Initiation Bypasses Signaling Crosstalk Mechanisms That Maintain High MYC Levels in Colorectal Cancer. Cancer Discov. 2015;5(7):768–81. [PubMed: 25934076]
27. Robert F, Roman W, Bramoulle A, Fellmann C, Roulston A, Shustik C, et al. Translation initiation factor eIF4F modifies the dexamethasone response in multiple myeloma. Proceedings of the National Academy of Sciences of the United States of America. 2014;111(37):13421–6. [PubMed: 25197055]
28. Rong L, Livingstone M, Sukarieh R, Petroulakis E, Gingras AC, Crosby K, et al. Control of eIF4E cellular localization by eIF4E-binding proteins, 4E-BPs. Rna. 2008;14(7):1318–27. [PubMed: 18515545]

29. Pettersson F, Del Rincon SV, Miller WH Jr. Eukaryotic translation initiation factor 4E as a novel therapeutic target in hematological malignancies and beyond. Expert Opin Ther Targets. 2014;18(9):1035–48. [PubMed: 25004955]
30. Yang T, Buchan HL, Townsend KJ, Craig RW. MCL-1, a member of the BLC-2 family, is induced rapidly in response to signals for cell differentiation or death, but not to signals for cell proliferation. J Cell Physiol. 1996;166(3):523–36. [PubMed: 8600156]
31. Raynaud FI, Orr RM, Goddard PM, Lacey HA, Lancashire H, Judson IR, et al. Pharmacokinetics of G3139, a phosphorothioate oligodeoxynucleotide antisense to bcl-2, after intravenous administration or continuous subcutaneous infusion to mice. J Pharmacol Exp Ther. 1997;281(1): 420–7. [PubMed: 9103525]
32. Pestova TV, Shatsky IN, Hellen CU. Functional dissection of eukaryotic initiation factor 4F: the 4A subunit and the central domain of the 4G subunit are sufficient to mediate internal entry of 43S preinitiation complexes. Mol Cell Biol. 1996;16(12):6870–8. [PubMed: 8943342]
33. Svitkin YV, Pause A, Haghighat A, Pyronnet S, Witherell G, Belsham GJ, et al. The requirement for eukaryotic initiation factor 4A (eIF4A) in translation is in direct proportion to the degree of mRNA 5' secondary structure. RNA. 2001;7(3):382–94. [PubMed: 11333019]
34. Chu J, Galicia-Vazquez G, Cencic R, Mills JR, Katigbak A, Porco JA Jr., et al. CRISPR-Mediated Drug-Target Validation Reveals Selective Pharmacological Inhibition of the RNA Helicase, eIF4A. Cell Rep. 2016;15(11):2340–7. [PubMed: 27239032]
35. Pelletier J, Graff J, Ruggero D, Sonenberg N. Targeting the eIF4F translation initiation complex: a critical nexus for cancer development. Cancer Res. 2015;75(2):250–63. [PubMed: 25593033]
36. Iwasaki S, Iwasaki W, Takahashi M, Sakamoto A, Watanabe C, Shichino Y, et al. The Translation Inhibitor Rocaglamide Targets a Bimolecular Cavity between eIF4A and Polypurine RNA. Mol Cell. 2018.
37. Iwasaki S, Floor SN, Ingolia NT. Rocaglates convert DEAD-box protein eIF4A into a sequence-selective translational repressor. Nature. 2016;534(7608):558–61. [PubMed: 27309803]
38. Chambers JM, Lindqvist LM, Webb A, Huang DC, Savage GP, Rizzacasa MA. Synthesis of biotinylated episilvestrol: highly selective targeting of the translation factors eIF4AI/II. Org Lett. 2013;15(6):1406–9. [PubMed: 23461621]
39. Andreou AZ, Klostermeier D. The DEAD-box helicase eIF4A: paradigm or the odd one out? RNA Biol. 2013;10(1):19–32. [PubMed: 22995829]
40. Oblinger JL, Burns SS, Akhmametyeva EM, Huang J, Pan L, Ren Y, et al. Components of the eIF4F complex are potential therapeutic targets for malignant peripheral nerve sheath tumors and vestibular schwannomas. Neuro Oncol. 2016;18(9):1265–77. [PubMed: 26951381]
41. Galicia-Vazquez G, Cencic R, Robert F, Agenor AQ, Pelletier J. A cellular response linking eIF4AI activity to eIF4AII transcription. Rna. 2012;18(7):1373–84. [PubMed: 22589333]
42. Chu J, Cencic R, Wang W, Porco JA Jr., Pelletier J Translation Inhibition by Rocaglates Is Independent of eIF4E Phosphorylation Status. Molecular cancer therapeutics. 2016;15(1):136–41. [PubMed: 26586722]
43. den Hollander J, Rimpi S, Doherty JR, Rudelius M, Buck A, Hoellein A, et al. Aurora kinases A and B are up-regulated by Myc and are essential for maintenance of the malignant state. Blood. 2010;116(9):1498–505. [PubMed: 20519624]
44. Ren Y, Bi C, Zhao X, Lwin T, Wang C, Yuan J, et al. PLK1 stabilizes a MYC-dependent kinase network in aggressive B cell lymphomas. J Clin Invest. 2018;128(12):5517–30. [PubMed: 30260324]
45. Malka-Mahieu H, Newman M, Desaubry L, Robert C, Vagner S. Molecular Pathways: The eIF4F Translation Initiation Complex-New Opportunities for Cancer Treatment. Clin Cancer Res. 2017;23(1):21–5. [PubMed: 27789529]
46. Lin CJ, Malina A, Pelletier J. c-Myc and eIF4F constitute a feedforward loop that regulates cell growth: implications for anticancer therapy. Cancer Res. 2009;69(19):7491–4. [PubMed: 19773439]
47. Cope CL, Gilley R, Balmanno K, Sale MJ, Howarth KD, Hampson M, et al. Adaptation to mTOR kinase inhibitors by amplification of eIF4E to maintain cap-dependent translation. J Cell Sci. 2014;127(Pt 4):788–800. [PubMed: 24363449]

48. Duncan R, Hershey JW. Identification and quantitation of levels of protein synthesis initiation factors in crude HeLa cell lysates by two-dimensional polyacrylamide gel electrophoresis. J Biol Chem. 1983;258(11):7228–35. [PubMed: 6853516]

49. Peters TL, Tillotson J, Yeomans AM, Wilmore S, Lemm E, Jimenez-Romero C, et al. Target-Based Screening against eIF4A1 Reveals the Marine Natural Product Elatol as a Novel Inhibitor of Translation Initiation with In Vivo Antitumor Activity. Clin Cancer Res. 2018;24(17):4256–70. [PubMed: 29844128]

50. Cencic R, Pelletier J. Hippuristanol - A potent steroid inhibitor of eukaryotic initiation factor 4A. Translation (Austin). 2016;4(1):e1137381. [PubMed: 27335721]

51. Bonetti P, Testoni M, Scandurra M, Ponzoni M, Piva R, Mensah AA, et al. Deregulation of ETS1 and FLI1 contributes to the pathogenesis of diffuse large B-cell lymphoma. Blood. 2013;122(13): 2233–41. [PubMed: 23926301]

52. Schmitz R, Ceribelli M, Pittaluga S, Wright G, Staudt LM. Oncogenic mechanisms in Burkitt lymphoma. Cold Spring Harb Perspect Med. 2014;4(2).

53. Lobry C, Oh P, Mansour MR, Look AT, Aifantis I. Notch signaling: switching an oncogene to a tumor suppressor. Blood. 2014;123(16):2451–9. [PubMed: 24608975]

54. Basso K, Dalla-Favera R. BCL6: master regulator of the germinal center reaction and key oncogene in B cell lymphomagenesis. Adv Immunol. 2010;105:193–210. [PubMed: 20510734]

55. Bi C, Zhang X, Lu T, Zhang X, Wang X, Meng B, et al. Inhibition of 4EBP phosphorylation mediates the cytotoxic effect of mechanistic target of rapamycin kinase inhibitors in aggressive B-cell lymphomas. Haematologica. 2017;102(4):755–64. [PubMed: 28104700]

56. Yueh H, Gao Q, Porco JA Jr., Beeler AB. A photochemical flow reactor for large scale syntheses of aglain and rocaglate natural product analogues. Bioorg Med Chem. 2017;25(23):6197–202. [PubMed: 28666859]

57. Stone SD, Lajkiewicz NJ, Whitesell L, Hilmy A, Porco JA Jr. Biomimetic kinetic resolution: highly enantio- and diastereoselective transfer hydrogenation of aglain ketones to access flavagline natural products. J Am Chem Soc. 2015;137(1):525–30. [PubMed: 25514979]

58. Rodrigo CM, Cencic R, Roche SP, Pelletier J, Porco JA. Synthesis of rocaglamide hydroxamates and related compounds as eukaryotic translation inhibitors: synthetic and biological studies. J Med Chem. 2012;55(1):558–62. [PubMed: 22128783]

59. Wang W, Cencic R, Whitesell L, Pelletier J, Porco JA Jr. Synthesis of Aza-Rocaglates via ESIPT-Mediated (3+2) Photocycloaddition. Chemistry. 2016;22(34):12006–10. [PubMed: 27338157]

60. Saradhi UV, Gupta SV, Chiu M, Wang J, Ling Y, Liu Z, et al. Characterization of silvestrol pharmacokinetics in mice using liquid chromatography-tandem mass spectrometry. AAPS J. 2011;13(3):347–56. [PubMed: 21499689]

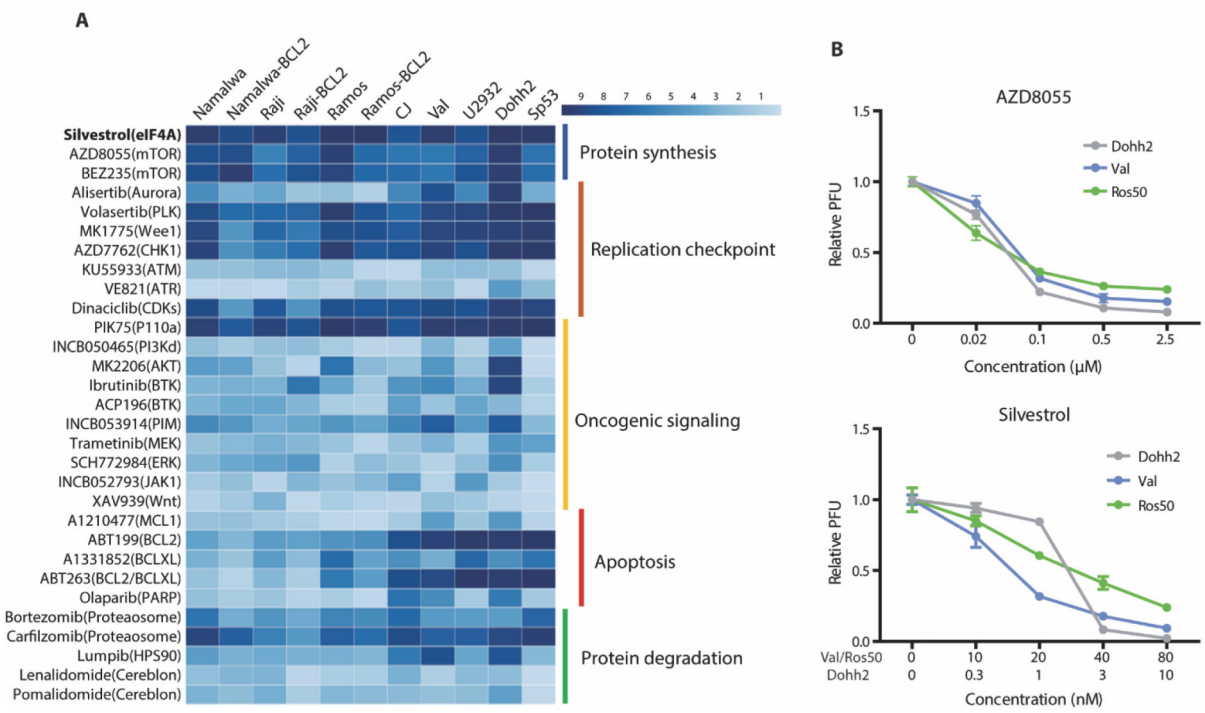

Figure 1.

Inhibitors targeting protein synthesis exhibit high potency in MYC-driven lymphomas. **a** Functional drug screens in MYC-driven lymphomas (Namalwa, Raji, Ramos, Namalwa-BCL2, Raji-BCL2, Ramos BCL2, CJ, Val, Dohh2, U2932 and Sp53). Small molecule inhibitors and corresponding targets are clustered according biology function and represented in an AUC heatmap format. AUC was calculated from concentration (μM) log-transformed dose-response curve of three independent experiments. **b** mTOR inhibitor AZD8055 and silvestrol decreased DHL cell viability. DHL cell Dohh2, Val and Ros50 were treated with AZD8055 or silvestrol at various concentrations. Cell viability was determined by prestoblue fluorescent unit (PFU) at 48 hours and normalized to vehicle control. Data presented show the mean ± SD of at least 3 independent experiments.

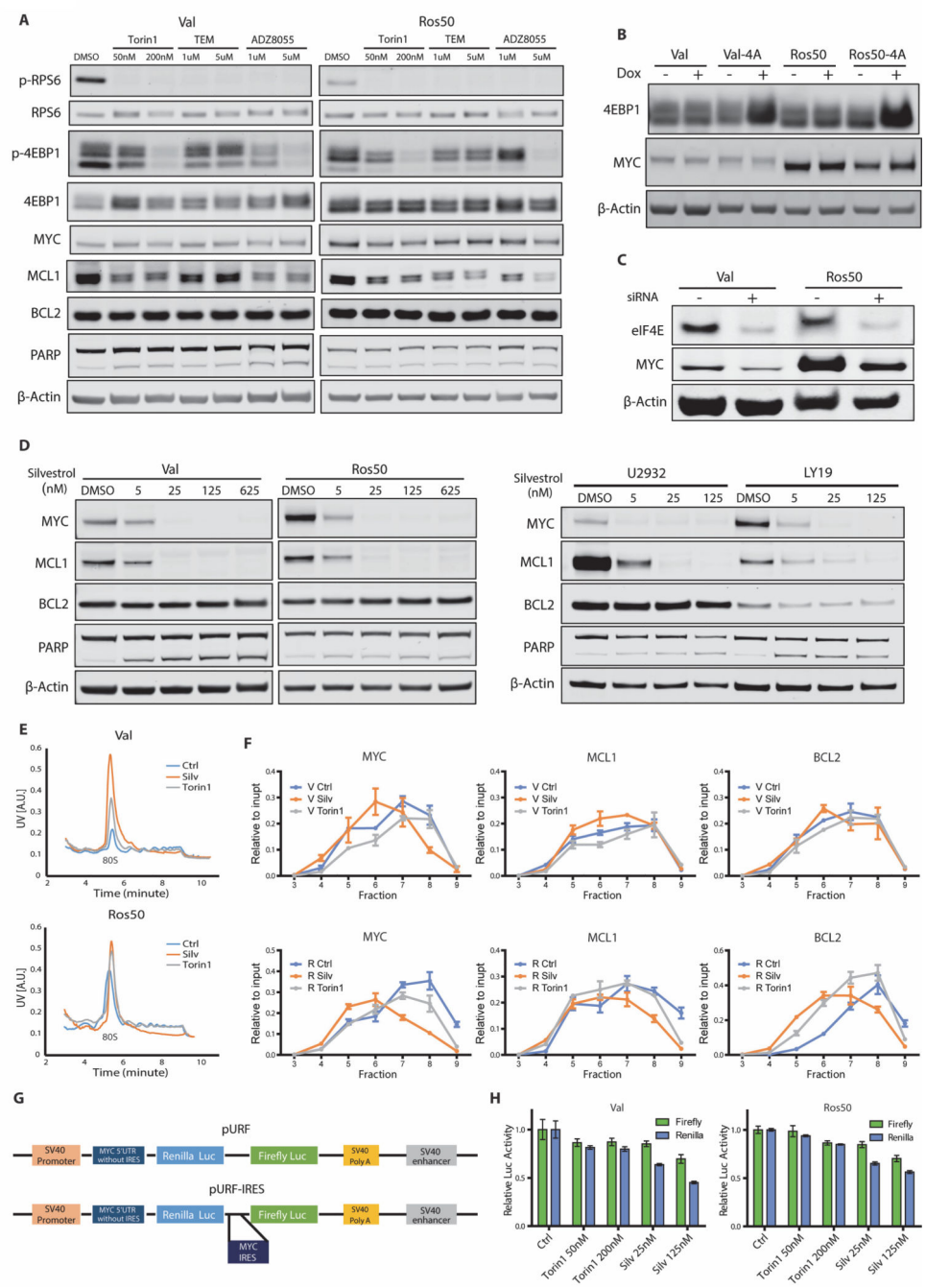

Figure 2.

Rocaglates but not mTOR inhibitors efficiently repress MYC expression. **a** Effect of mTOR inhibitors on oncoprotein MYC, MCL1 and BCL2. Val and Ros50 cells treated with Torin1, temsirolimus (TEM) and AZD8055 at indicated concentrations for 24 hours. Protein levels were examined by immunoblotting. **b** 4EBP1–4A was introduced into Val and Ros50 cells by retrovirus infection and the ectopic expression was induced by doxycycline (1 μg/ml) for 48 hours. **c** siRNA targeting eIF4E was transfected into Val and Ros50 cells by electroporation. MYC protein level was determined at 48 hours post-transfection. **d** DHL

cell lines Val and Ros50, and DEL cell lines U2932 and LY19 were treated with increasing concentrations of silvestrol for 24 hours. MYC, MCL1, BCL2 and PARP were measured by immunoblotting. **e** Polysome fractionations were plotted (260nM absorbance) in Val and Ros50 cells treated with 200nM Torin1, 125nM Silvestrol (Silv) or vehicle control for 2 hours. Collection was set at one fraction per minute. **f** Distribution of MYC, MCL1 and BCL2 mRNA was measured in each fraction. Relative mRNA content per fraction was measured by RT-qPCR. **g** Schematic illustration describing luciferase reporters used in this study. pURF contains IRES element deleted MYC 5'UTR inserted proximal to renilla luciferase coding sequence. pURF-IRES was generated by inserting MYC-IRES element in front of firefly luciferase coding sequence in pURF construct. **h** Val and Ros50 cells transduced with pURF-IRES were treated with Torin1 or silvestrol (Silv) for 4 hours. Luciferase activity was measured and normalized to cell number and that of vehicle control. Data in **a-e** shown are representative of at least 3 independent experiments. Data presented in **h** show the mean ± SD of at least 3 independent experiments.

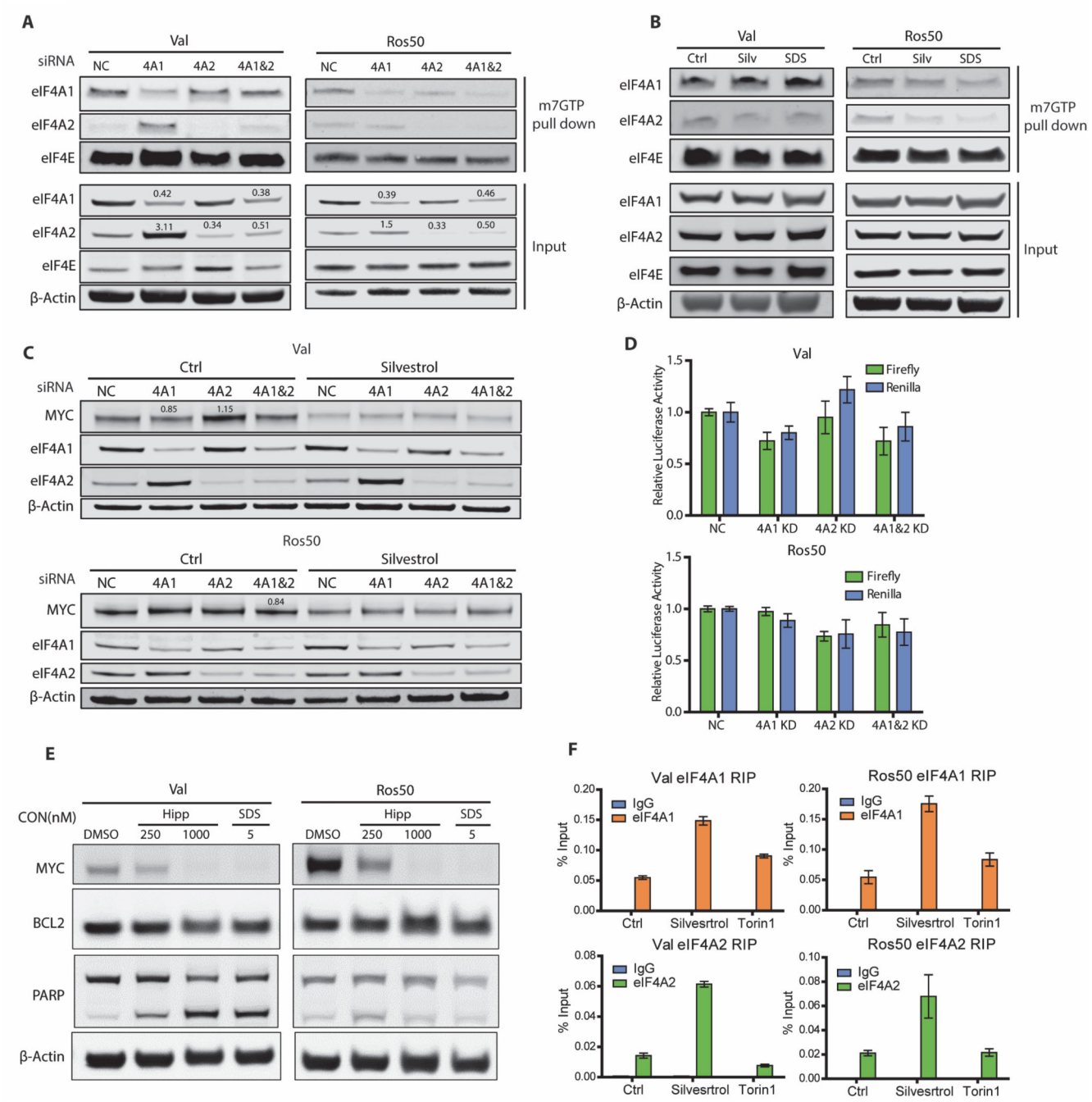

Figure 3.

Rocaglates increase MYC mRNA binding to eIF4A, instead of depleting eIF4A in eIF4F. **a** Evaluation of total eIF4A1 and eIF4A2 as well as their abundance in eIF4F following siRNA knockdown in Val and Ros50 cells. Knockdown efficiency indicated in lane. **b** Evaluation of eIF4A1 and eIF4A2 abundance in eIF4F after 4 hours treatment with 125nM silvestrol (Silv), 100 nM (-)-SDS-1-021(SDS) or vehicle control in Val and Ros50 cells. **c** Alterations of MYC expression after eIF4A1, eIF4A2 or combined knockdown, and with silvestrol added. siRNA transfected Val and Ros50 cells were incubated with vehicle control

or silvestrol (125 nM) for 4 hours. **d** Dual luciferase assay performed in eIF4A knock down cells. Luciferase activity measured at 48 hours post-transfection and normalized to cell number. **e** eIF4A inhibitor hippuristanol (Hipp) and (−)SDS-1–021 (SDS)(24 hours) induced reduction of MYC protein. **f** Native RNA immunoprecipitation measuring MYC mRNA enrichment on eIF4A1 and eIF4A2. Data shown in **a**, **b**, **c** and **e** are representative of at least 3 independent experiments. Data presented in **d** and **f** show the mean ± SD of at least 3 independent experiments.

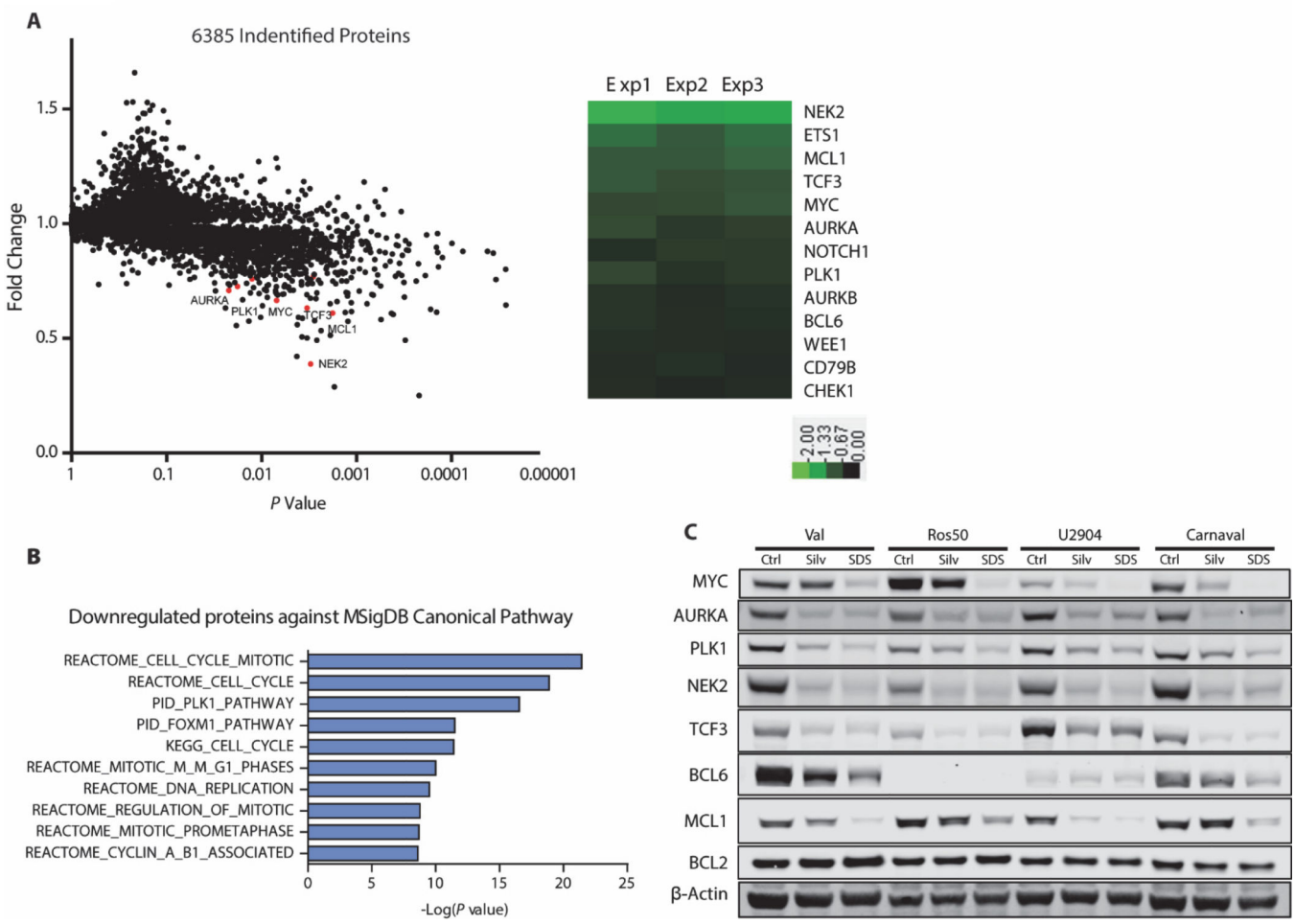

Figure 4.

Rocaglates repress multiple critical oncoproteins in DHL/DEL. **a** Quantitative proteomics demonstrating the impact of (-)-SDS-1-021 treatment (100 nM) relative to vehicle control in Val cells after 4-hour incubation (three biological replicates TMT labelled). Totally, 6385 proteins were identified, of which 177 were significantly depleted for more than 20% by (-)-SDS-1-021 ($P < 0.05$). Depleted critical oncoproteins in B cell lymphoma are highlighted and presented as heatmap ($\log_2$ transformation of relative abundance ratio). **b** Enriched pathways identified by querying the 177 depleted proteins in MSigDB C2 canonical pathway database. **c** Val, Ros50, U2904 and Carnaval cells were treated with vehicle control, silvestrol (25nM) or (-)-SDS-1-021 (25nM) for 24 hours and validated the expression of the target oncoproteins by immunoblotting. Data shown are representative of at least 3 independent experiments.

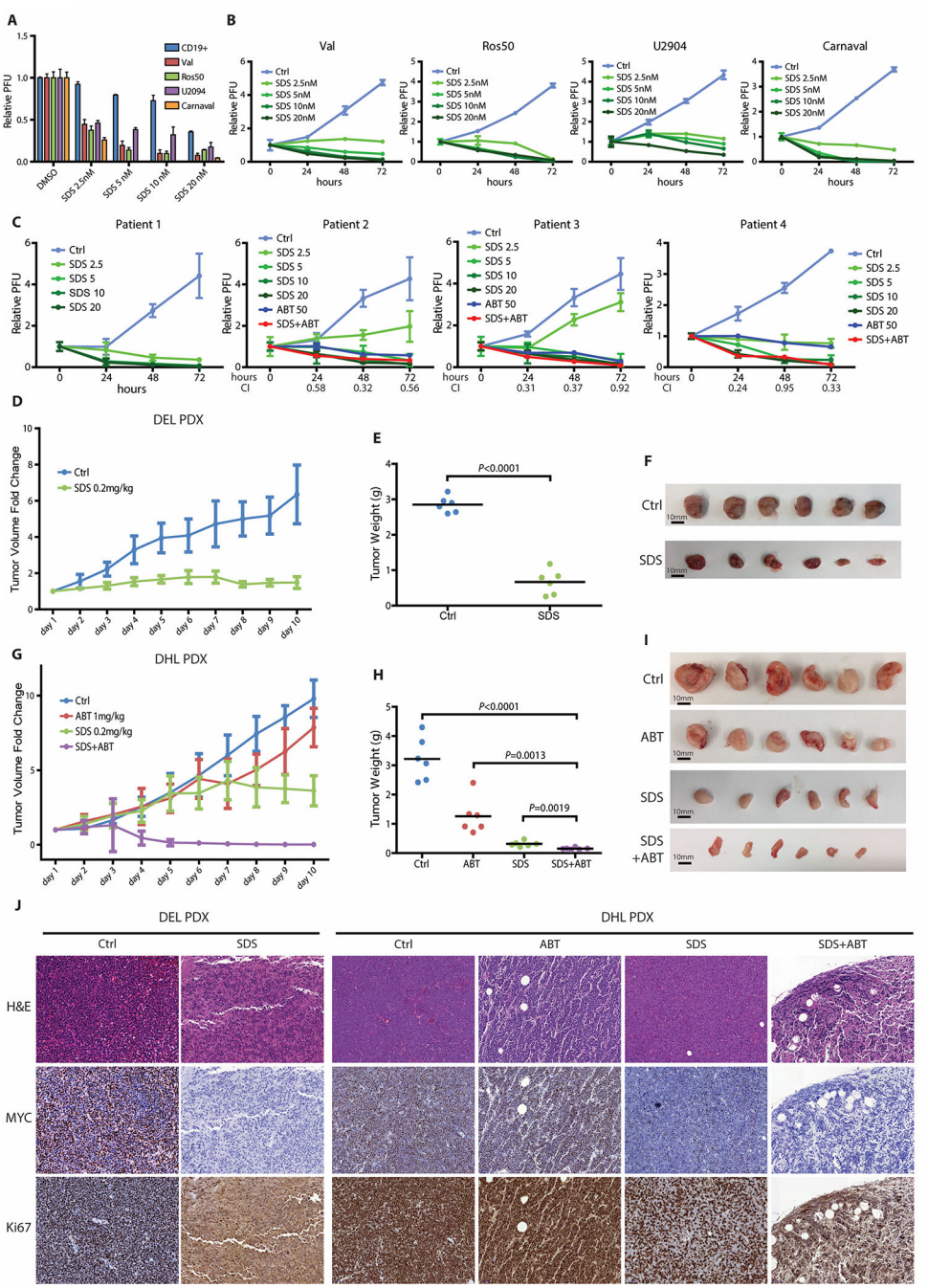

Figure 5.

(-)-SDS-1-021 exhibits promising therapeutic effect, and synergizes with ABT199 *in vitro* and *in vivo*. **a** Impact of (-)-SDS-1-021(SDS) on normal CD19+ B cell and DHL/DEL cell viability at 48 hours. PFU in treated cells was normalized to vehicle control. **b** Impact of (-)-SDS-1-021(SDS) on DHL/DEL cell proliferation. PFU in treatment groups was normalized to day 0. **c** Efficacy of (-)-SDS-1-021, ABT199 (50 nM) and combined treatment (2.5nM SDS+ 50 nM ABT199) in primary DEL/DHL lymphoma cells. PFU was normalized to day 0. Combination index (CI) is calculated and indicated as the value less than 1 suggesting

synergistic effect between two drugs. **d** Tumor growth of a double expression lymphoma (DEL) model in NSG mice. (-)-SDS-1-021(0.2mg/kg) or vehicle control was administered by intraperitoneal (i.p.) injections daily for 10 days. **e** Weight of tumor from vehicle control or (-)-SDS-1-021 treated DEL PDX mice at endpoint. $P<0.0001$. **f** Representative images of the tumors from DEL PDX therapeutic study shown in **d** and **e**. **g** Tumor growth of double hit lymphoma (DHL) in NSG mice. (-)-SDS-1-021(0.2 mg/kg), ABT199 (1 mg/kg), combined treatment or vehicle control was administered by i.p. injections daily for 10 days. **h** Weight of tumor from vehicle control or therapeutic groups DHL PDX mice at endpoint. *P* value between combined and control group ($P<0.0001$), ABT199 group ($P=0.0013$), or (-)-SDS-1-021 group, ($P=0.0019$). **i** Representative images of the tumors from DHL PDX therapeutic study shown in **g** and **h**. **j** IHC staining of MYC and Ki67 in DEL and DHL PDX models. Original magnification ×200. Data shown in **a**-**c** represent mean ± SD of at least 3 independent experiment. Results are shown as mean ± SD of 6 animals/group for **d** and **g**.